B-CLEAN-SC: CLEAN-SC for broadband sources

Armin Goudarzi ⓘ

Check for updates

View Online

Export Citation

CrossMark

B–CLEAN–SC: CLEAN–SC for broadband sources

Armin Goudarzi[a] iD
German Aerospace Center (DLR), 37073 Göttingen, Germany
armin.goudarzi@dlr.de

Abstract: This paper presents B-CLEAN-SC, a variation of CLEAN-SC for broadband sources. In contrast to CLEAN-SC, which "deconvolves" the beamforming map for each frequency individually, B-CLEAN-SC processes frequency intervals. Instead of performing a deconvolution iteration at the location of the maximum level, B-CLEAN-SC performs it at the location of the over-frequency-averaged maximum to improve the location estimation. The method is validated and compared to standard CLEAN-SC on synthetic cases and real-world experiments for broad- and narrowband sources. It improves the source reconstruction at low and high frequencies and suppresses noise, while it only increases the need for memory and not computational effort. © 2023 Author(s). All article content, except where otherwise noted, is licensed under a Creative Commons Attribution (CC BY) license (http://creativecommons.org/licenses/by/4.0/).

1. Introduction

Conventional beamforming is a well-established tool to identify and quantify sound sources on complex objects, such as cars, trains, and aircrafts (Merino-Martínez *et al.*, 2019). Naive methods estimate the sound power by virtually steering the cross spectral matrix (CSM) to different focus points to obtain an independent estimation for each focus point. The resulting beamforming map is convoluted with the array's point spread function (PSF), which limits the resolution at low frequencies by the array's aperture and at high frequencies by aliasing that results from the discrete microphone spacing. More advanced methods exist, such as gridless methods (Chardon, 2023; Goudarzi, 2023; Kujawski and Sarradj, 2022; Sarradj, 2022). However, they are computationally expensive and often only proven to work on academic examples.

There exist a variety of "deconvolution" methods that aim to reconstruct the true source distribution from the so-called dirty beamforming maps. While advanced source reconstruction methods such as DAMAS (Brooks and Humphreys, 2006; Chardon *et al.*, 2021; Ehrenfried and Koop, 2007) exist, CLEAN-SC (Sijtsma, 2007) is the gold standard in industrial environments (Ahlefeldt, 2017; Ahlefeldt *et al.*, 2023) because it is fast and robust.

CLEAN-SC solves the deconvolution iteratively at each individual frequency. It assumes a dominant source per iteration so that the dirty map is dominated by its PSF. It then estimates that the source is located at the location of maximum power spectral density (PSD) in the map and measures the coherence between the location and all other locations. It then subtracts the source from the CSM and dirty map. It then repeats the process to find additional sources until a stopping criterion is met. This process works well for spatially compact sources (Merino-Martínez *et al.*, 2020) at medium frequencies, where the PSF shows pronounced mainlobes and low sidelobes. At low frequencies (compared to the array's aperture), the PSF of two adjacent sources will overlap and form a single blob in the dirty map. Thus, the maximum of the dirty map is no longer located at a true source position, but between multiple source positions. At these low frequencies, CLEAN-SC fails to identify the true sources and reconstructs the PSD wrongly. At high frequencies, the focus grid can often no longer resolve the mainlobe. Additionally, grating-lobes are present in the dirty map that are of the same magnitude as the mainlobe. Thus, the maximum is often positioned at a grating-lobe, which results in noisy CLEAN-SC maps at these high frequencies. The improved algorithm HR-CLEAN-SC (Sijtsma *et al.*, 2017) aims to solve the low-frequency issues of CLEAN-SC, which requires an initial CLEAN-SC solution and an additional iteration to obtain a solution. The spatial resolution of HR-CLEAN-SC is approximately doubled compared to CLEAN-SC, but less so if diagonal removal (DR) is applied.

Recently, a variation of the gridless CSM-fitting method global optimization (GO) was introduced for broadband sources (Goudarzi, 2023; Malgoezar *et al.*, 2017) based on the observation that sources typically have a constant location over frequency (Goudarzi *et al.*, 2021). Broadband GO showed that introducing the condition of a shared location over frequency smooths out local minima in the optimization cost function, which are caused by the side- and grating-lobes of the array's PSF. While the results were superior compared to CLEAN-SC and standard GO, the computational effort makes the method currently not suitable for industry applications (Chardon, 2023; Goudarzi, 2023).

---

[a] Author to whom correspondence should be addressed.

This paper introduces broadband-CLEAN-SC (B-CLEAN-SC), which aims to relax the problems of CLEAN-SC at high and low frequencies by adapting the idea of broadband GO: the processing of multiple frequencies at once, so that the sidelobes cancel out and true source positions can be identified. This is done by introducing a simple change to the CLEAN-SC algorithm: Instead of processing each frequency individually, B-CLEAN-SC processes frequency intervals at once (but still obtains smallband solutions). Here, the only difference lies in the determination of the location, from which the source power is sampled. B-CLEAN-SC averages the dirty maps over the frequency interval and uses the location of the maximum averaged source power. It then performs a standard CLEAN-SC iteration for each of the frequencies in the interval with individual source powers per frequency but at the shared location. Thus, the reconstruction at lower frequencies benefits from the resolution at higher frequencies, and the averaging of side- and grating-lobes stabilizes the process at high frequencies.

2. Methodology

This section presents the standard CLEAN-SC algorithm and the proposed B-CLEAN-SC algorithm.

2.1 Standard CLEAN-SC

CLEAN-SC is based on the idea that the coherence Γ_{jk}^2 between an arbitrary focus point $\mathbf{x}_k$ and all other focus points $\mathbf{x}_j$ can be estimated by steering the CSM to the focus points with

$$\Gamma_{jk}^2 = \frac{|\mathbf{w}_j^* \mathbf{C} \mathbf{w}_k|^2}{(\mathbf{w}_j^* \mathbf{C} \mathbf{w}_j)(\mathbf{w}_k^* \mathbf{C} \mathbf{w}_k)} = \frac{|A_{jk}|^2}{A_{jj} A_{kk}} , \tag{1}$$

where w is an arbitrary steering vector (Sarradj, 2012), and $(\cdots)^*$ denotes the Hermetian transpose. Removing the coherent parts of a source removes the PSF (but also distributed sources) from the map. This is performed iteratively with Algorithm 1, where n is the current iteration, for a maximum number of N iterations, or until a stopping criterion is met (Sijtsma, 2007), $f \in \mathbf{f}$ is the current frequency, $\mathbf{f} = [f_1, f_2, \ldots]$ is a frequency vector, A is the conventional beamforming result for the steering vector w, x is a list of all focus points, C is the dirty CSM, G is the CSM of the iteratively identified source, and Q is the final CLEAN-SC estimation of the "deconvolved" map. For stability, a loop gain $0 < \alpha \le 1$ is used. CLEAN-SC can be performed with DR by iteratively adjusting the steering vectors, where I is the identity matrix and $\circ$ is the Hadamard product in the algorithm.

Algorithm 1. Standard CLEAN-SC.

FUNCTION CLEAN-SC $(\mathbf{C}, \mathbf{w}, \alpha)$:
$\mathbf{Q}(\mathbf{f}, \mathbf{x}) \leftarrow \mathbf{0}$
for f in f do
  $n \leftarrow 0$
  $\mathbf{A}_{jj} \leftarrow \mathbf{w}_j^*(f) \mathbf{C}(f) \mathbf{w}_j(f)$
  while $n \le N$ **do**   {or another arbitrary stopping criterion is met}
    $n \leftarrow n + 1$
    $k \leftarrow \text{argmax}_j(\mathbf{A}_{jj})$
    $A_{kk} \leftarrow \mathbf{A}_{jj}(\mathbf{x}_k)$ {find pos. of max. amplitude}
    $\mathbf{h} \leftarrow \dfrac{\mathbf{C}(f) \mathbf{w}_k(f)}{A_{kk}}$ {find steering vector to the corresp. loc.}
    if DR then
      $\mathbf{H} \leftarrow \mathbf{I} \circ \mathbf{h}\mathbf{h}^*$ {diag. matrix from steering vector}
      $\mathbf{h} \leftarrow \dfrac{1}{1 + \mathbf{w}^* \mathbf{H} \mathbf{w}} \left(\dfrac{\mathbf{C}(f) \mathbf{w}}{\mathbf{w}^* \mathbf{C}(f) \mathbf{w}} + \mathbf{H} \mathbf{w} \right)$ {iteratively find steering vector if DR}
    end if
    $\mathbf{G} \leftarrow A_{kk} \mathbf{h}\mathbf{h}^*$ {calc. CSM for the identified source}
    $\mathbf{C}(f) \leftarrow \mathbf{C}(f) - \alpha \mathbf{G}$ {subtract identified source from dirty CSM}
    $\mathbf{A}_{jj} \leftarrow \mathbf{A}_{jj} - \alpha \mathbf{w}_j^*(f) \mathbf{G}(f) \mathbf{w}_j(f)$ {subtract corresponding beamforming result from dirty map}
    $\mathbf{Q}(f, \mathbf{x}_k) \leftarrow \mathbf{Q}(f, \mathbf{x}_k) + \alpha A_{kk}$ {add identified source strength to CLEAN-SC output}
  end while
end for
return $\mathbf{Q}(\mathbf{f}, \mathbf{x})$

2.2 B-CLEAN-SC

The B-CLEAN-SC algorithm is nearly identical to the CLEAN-SC algorithm, when CLEAN-SC is performed for all frequencies in parallel with the exception that B-CLEAN-SC performs each iteration n at a shared location $\mathbf{x}_k$ for all frequencies (within the processed interval f). To determine the location, instead of using the maximum of the dirty map $\mathbf{A}_{jj}(f)$ separately for each frequency, the maximum of the over-frequency-averaged dirty map is used,

$$k = \mathrm{argmax}_j \left(\left\langle \frac{\mathbf{A}_{ijj}}{\max_j(\mathbf{A}_{ijj}^0)} \right\rangle_i \right). \tag{2}$$

Here, $\mathbf{A}_{ijj}^0$ denotes the original dirty map prior to subtractions. i denotes the index of the frequency $f_i \in \mathbf{f}$, and j denotes the index of the focus point $\mathbf{x}_j$. The subscript of the average operator $\langle \cdots \rangle$ or the maximum argument operator indicates the dimension over which they are applied. $\mathbf{A}_{ijj}^0$ is an estimation for the frequency-dependent amplitude of the overall source power (which typically decreases over frequency for aeroacoustic sources). The normalization by its maximum compensates for this behavior. Equation (2) is the only addition to the CLEAN-SC algorithm to obtain B-CLEAN-SC (see Algorithm 2). The algorithm is given for a frequency interval f; if the frequency interval does not cover the full frequency range, B-CLEAN-SC is performed sequentially for multiple intervals.

   Note that the position $\mathbf{x}_k$ is not necessarily located on the mainlobe of a dominant source for all frequencies if the sources have a strong frequency-dependent power. Especially at low frequencies, where the PSF of a dominant source may cover all other sources and dominate the estimated power at their true positions, this would lead to an overestimation of their power, and a subtraction of the mainlobe, when subtracting coherent portions of the map (Sijtsma *et al.*, 2017). To relax this issue, a low gain factor α is needed, so that the number of necessary B-CLEAN-SC iterations increases. Since only the initial calculation of the dirty map is computationally expensive, the extra iterations are not performance relevant.

3. Results

This section presents three different cases. Section 3.1 presents a synthetic example that aims to clarify the behavior of CLEAN-SC and B-CLEAN-SC. Section 3.2 presents an open wind tunnel experiment with ground truth, so that the methods can be evaluated quantitatively. Last, Sec. 3.3 presents a closed wind tunnel experiment without ground truth, based on which the methods are evaluated qualitatively. Throughout this section, CLEAN-SC will be performed with DR, a maximum of $3N_S$ iterations per frequency, where NS is the number of true sources, and a gain factor of $\alpha = 0.9$ per iteration. B-CLEAN-SC will be performed with DR, a maximum of $10N_S$ iterations, and $\alpha = 0.1$ per iteration. To reduce the visual complexity of the results, beamforming maps are obtained only in one dimension for case 1 and two dimensions for cases

Algorithm 2. B-CLEAN-SC for a frequency interval f.

```
FUNCTION B-CLEAN-SC (C, w, α):
Q ← 0
n ← 0
A⁰ᵢⱼⱼ ← w*ᵢⱼ Cᵢ wᵢⱼ
while n ≤ N do
    n ← n + 1
    Âⱼⱼ ← ⟨ Aᵢⱼⱼ / maxⱼ(A⁰ᵢⱼⱼ) ⟩ᵢ
    k ← argmaxⱼ(Âⱼⱼ)      {change to the CLEAN-SC algorithm}
    Aᵢₖₖ ← Aᵢⱼⱼ(xₖ)
    hᵢₖ ← Cᵢ wᵢₖ / Aᵢₖₖ
    if DR then
        Hᵢₖₖ ← hᵢₖ h*ᵢₖ Iₖₖ
        hᵢₖ ← 1/(1 + w*ᵢₖ Hᵢₖₖ wᵢₖ) ( Cᵢ wᵢₖ / w*ᵢₖ Cᵢ wᵢₖ + Hᵢₖₖ wᵢₖ )
    end if
    Gᵢ ← Aᵢₖₖ hᵢₖ h*ᵢₖ
    Cᵢ ← Cᵢ − α Gᵢ
    Aᵢⱼⱼ ← Aᵢⱼⱼ − α w*ᵢⱼ Gᵢ wᵢⱼ
    Q(fᵢ, xₖ) ← Q(fᵢ, xₖ) + α Aᵢₖₖ
end while
return Q(f, x)
```

2 and 3 with steering vector formulation III (Sarradj, 2012). The results will be presented over the Helmholtz number He $= fD/a$, where D is the array's aperture, and a is the speed of sound.

3.1 Synthetic results

Case 1 is a synthetic one-dimensional (1D) example that highlights the differences between standard CLEAN-SC and B-CLEAN-SC. The array is located at $-0.5 \leq x \leq 0.5$, y $= 0$. There are three sources Si at $x_1 = 0$, $x_2 = 0.1$, $x_3 = 0.5$, y $= 0.5$. The CSM is calculated at 256 frequencies, $f_{max} = 8192$ Hz, $\Delta f = 32$ Hz. The focus grid is located at $-1 \leq x \leq 1$, y $= 0.5$, $\Delta x = 0.004$ m. The PSD of S1 linearly increases over frequency from $PSD_1(f_0) = -10$ dB to $PSD_1(f_{256}) = 0$ dB. The PSD of S2 linearly decreases in the same way so that S2 dominates at low frequencies and S1 dominates at high frequencies. Additionally, S3 is a smallband source that is only present at 3616 Hz $\leq f \leq$ 3840 Hz at -10 dB. For B-CLEAN-SC, the frequencies are processed in intervals of $\Delta f = 2048$ Hz.

Figure 1 shows the results of case 1. Figures 1(e) and 1(f) show the estimated PSD, integrated from the same colored region of interest (ROI) in Figs. 1(a) and 1(d). The black lines represent noise, integrated from the area that does not correspond to any ROI indicating beamforming and deconvolution artifacts. Additionally, a magenta line shows the integration of all sources within the map, as an estimation of the overall sound power. The ground truth is depicted with dotted lines for reference.

CLEAN-SC reconstructs the dominant source S2 well down to He ≥ 0.8, below which the maximum within the dirty map is estimated with a wrong level along the sidelobes and then at the edges of the focal range. For S1, the PSD reconstruction works well down to He ≥ 4, below which CLEAN-SC gradually underestimates its power and gradually misses the correct location. The smallband source S3 is reconstructed perfectly. B-CLEAN-SC perfectly estimates the sources' locations. The PSDs are reconstructed well throughout the frequency range, except for an underestimation of S1 at He ≈ 3. For B-CLEAN-SC, there is no noise.

3.2 Experiment with ground truth

Case 2 is a generic open wind tunnel experiment at Mach (M) $= 0.06$ with a streamlined monopole speaker that is moved to three different locations (Goudarzi, 2023; Goudarzi et al., 2021) with different spectra and known ground truth. The sources are located at $x_1 = -0.05$, $x_2 = 0.1$, $x_3 = 0.25$, $y_{1,2,3} = 0.1$, $z_{1,2,3} = 0$. The array consists of 7×7 equidistantly spaced microphones with $\Delta x = \Delta y = 0.09$ m and is located at $z = -0.65$ outside of the flow. The equidistant two-dimensional (2D) focus grid $\Delta x = \Delta y = 0.005$ m covers $-0.3 \leq x, y \leq 0.3$ at z $= 0$. The sampling rate is $f_s = 65\,536$ Hz, and $\Delta f = 512$ Hz.

Figure 2 shows the results for case 2. Figures 2(a) and 2(d) show that CLEAN-SC results in noisier OASPL maps than B-CLEAN-SC. When integrating the maps over x, Figs. 2(b) and 2(e) show that CLEAN-SC is able to determine the correct location down to He ≈ 3. B-CLEAN-SC correctly determines throughout the frequency range. Strong sidelobes are reconstructed as "ghost sources" that move closer to the true source position with increasing frequency. Figures 2(c) and 2(f) show the spectrum estimation. Source S1 is estimated well by CLEAN-SC at He ≥ 8. Source S2 is estimated well down to He ≈ 1.5, below which it can no longer be separated from S3, estimated well down to He ≥ 2. Below this frequency, the overall power was estimated well but could not be attributed to a true source position, so it was
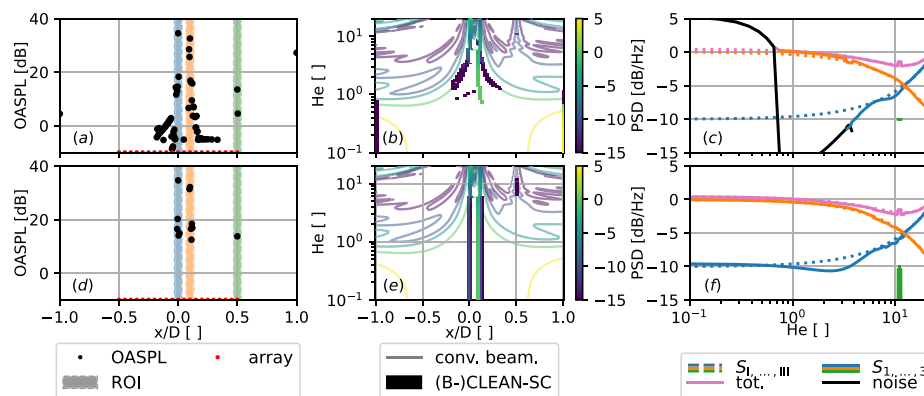

Fig. 1. Case 1: The top row shows CLEAN-SC results, and the bottom row shows B-CLEAN-SC results. (a) and (d) show the overall sound pressure level (OASPL)(x/D), integrated over all frequencies. The sensor positions are marked at an arbitrary y-location. The shaded areas represent the ROIs. (d) and (e) show the conventional beamforming result and the sparse (B-)CLEAN-SC result; the color indicates the PSD. (e) and (f) show the resulting spectra, integrated from the ROIs in (a) and (d). The sources are depicted with different colors: S1 (blue), S2 (orange), S3 (green), and the total integrated power (magenta). (B-)CLEAN-SC results that are not located within any ROI are spatially integrated and classified as noise (black). The ground truth is depicted with dotted lines and Roman numbers, and the ROI estimation is shown with full lines and Arabic numbers.
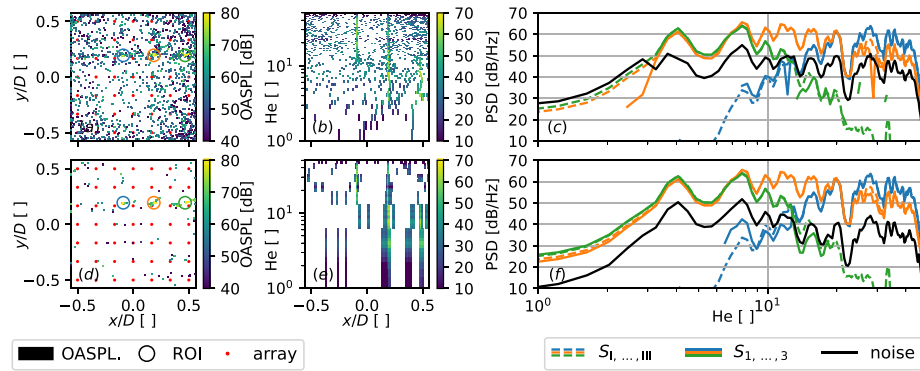
Fig. 2. Case 2: The top row shows CLEAN-SC results, and the bottom row shows B-CLEAN-SC results. (a) and (d) show the OASPL$(x/D, y/D)$ with colored ROI centered around the true source locations; (b) and (e) show the PSD$(x/D, f)$ integrated over the y-dimension; and (c) and (f) show the ground truth (dotted, Latin numbers) and estimated PSD (solid, Arabic numbers) from the identical colored ROI in (a) and (d). The black line represents noise, integrated from the areas that do not correspond to any ROI.

integrated as noise. Both S1 and S3 are reconstructed down a signal-to-signal ratio (SSR) of around SSR = 30 dB, which was used as an iteration stopping criterion. B-CLEAN-SC shows similar results, with improved reconstructions of S2 and S3 and lower levels of noise.

Table 1 shows a comparison of three different metrics for exemplary frequency intervals, where $|\cdots|$ is the absolute value, $||\cdots||$ is the number of elements, and $\langle\cdots\rangle_v$ is the average over the variable v. The relative frequency interval of the PSD that is correct [within a ± 3 dB margin of the ground truth (GT)] is defined for multiple sources S as

$$\text{corr.PSD} = \left\langle \frac{||-3 \leq |\text{PSD}(S,f) - \text{GT}(S,f)| \leq 3||_f}{||\text{PSD}(S,f)||_f} \right\rangle_S, \tag{3}$$

the mean absolute error (for frequencies where the PSD is defined, so that PSD $\neq -\infty$ dB),

$$\text{mean error} = \langle\langle|\text{PSD}(f) - \text{GT}(f)|\rangle_f\rangle_S, \tag{4}$$

and the SNR is the ratio of the maximum source level to the noise level (for frequencies where both are defined),

$$\text{SNR} = \langle\max_S(\text{PSD}(S,f)) - \text{noise}(f)\rangle_f. \tag{5}$$

Note that Eqs. (4) and (5) are conditional errors, since they require a defined PSD estimation. Figures 2(c) and 2(f) show that this is not always the case, so that they must be evaluated as subsidiary results of Eq. (3), e.g., the low-frequency CLEAN-SC noise is not captured with the SNR metric, as no signal is present. Table 1 shows that B-CLEAN-SC outperforms CLEAN-SC with an increasing frequency interval, with an optimum at $16 \leq ||\mathbf{f}|| \leq 32$. The SNR further improves with an increasing frequency interval, which indicates an improvement in the spatial localization, but the spectral estimation deteriorates in return.

3.3 Wind tunnel experiment

Case 3 is a closed wind tunnel measurement of a Dornier 728 (Do728) at M = 0.125 (Ahlefeldt, 2013). The 2D focus grid $\Delta x = \Delta y = 0.01$ m is rotated so that it covers and follows the wing. The spiral array with $D = 1$ m consists of 149 microphones and is located approximately $\Delta z = 1$ m from the wing. The signal is sampled at $f_s = 120$ kHz, and the CSM is sampled for 128 frequencies at $\Delta f \approx 479$ Hz. Since there exists no ground truth, the results will be discussed only qualitatively.

Figures 3(a) and 3(d) show the estimated OASPL $(x/D, y/D)$. The results correspond well to the geometric features of the wing, but CLEAN-SC shows noise in the top right corner, and sources such as the flap side edge are not well

TABLE 1. Influence of the frequency interval $\mathbf{f}$ on the resulting error metrics, where $||\mathbf{f}|| = 128$ are all frequencies.

$||\mathbf{f}||$	1[a]	2	4	8	16[b]	32	64	128
Correct PSD (%)	61.7	62.8	62.5	65.6	**66.7**	**66.7**	66.1	64.8
Mean error (dB)	2.3	2.2	2.5	2.5	**1.3**	2.5	3.9	8.9
SNR (dB)	14.5	14.4	14.8	16.4	17.8	18.4	**22.6**	19.1

[a]Corresponds to the CLEAN-SC result in Fig. 2, all with DR, $\alpha = 0.1$, $N = 30$.
[b]Corresponds to the B-CLEAN-SC result, all with DR, $\alpha = 0.1$, $N = 30$.
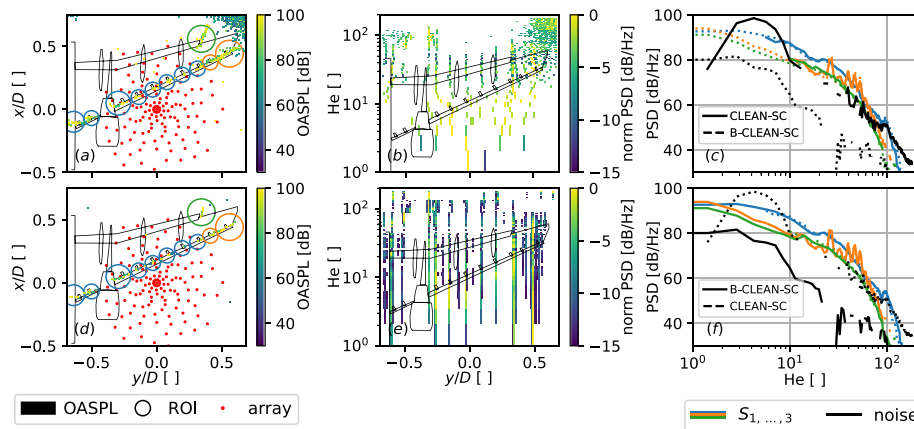
Fig. 3. Case 3: The top row shows CLEAN-SC results, and the bottom row shows B-CLEAN-SC results. (a) and (d) show the OASPL($x/D, y/D$); (b) and (e) show the normalized PSD($y/D, f$) integrated over the x-dimension and normalized per frequency. The model is depicted for reference (but its x-information should be ignored). (c) and (f) show the estimated PSD from the identical colored ROI in (a) and (d). While (c) shows the CLEAN-SC results (solid), the B-CLEAN-SC solution is displayed with dotted lines, and in (f) vice versa for comparison. Black lines indicate noise.

localized. Figures 3(b) and 3(e) show the PSD(y, f), integrated over x and normalized per frequency. Thus, the only sources that can be confused in this depiction are an outboard slat track and the flap side edge at $y/D \approx 0.3$. The model is depicted for reference, so that the estimated sources can be attributed to its geometrical features, such as the slat tracks. Note that the x-component of the model is plotted along the frequency axis, but the color-map does not include any x-information. Within the CLEAN-SC result, one can clearly identify slat tracks in a frequency range of $10 \leq He \leq 100$. Otherwise, the result mostly shows the inboard Krüger slat, the nacelle area, and the noise for $y/D \geq 0.5$. Below $He \leq 10$, the source separation fails. The B-CLEAN-SC result shows the same slat tracks as dominant sources. However, they are also reconstructed at low and high frequencies. Additionally, there is nearly no noise for $y/D \geq 0.5$. Additional sources are visible between the slat tracks, which are typically connected to slat cove tones (Goudarzi, 2022). Overall, the location of the estimated sources strongly correlates to the geometrical features of the model and is consistent over the whole frequency range.

Based on the analysis of these data (Goudarzi, 2022), ROIs are defined that cover the inner (Krüger) slat and the slat tracks (blue), the outer slat (orange), and the flap side edge (green). The ROIs are chosen so that the integrated source types are similar (Ahlefeldt *et al.*, 2023; Goudarzi, 2022). Figures 3(a) and 3(d) show the (identical) ROI, and Figs. 3(c) and 3(f) show the corresponding PSD. Below $He \leq 10$, CLEAN-SC fails to reconstruct individual sources, which results in strong noise, additional to the noise $He \geq 40$. B-CLEAN-SC reconstructs the PSD throughout the frequency range with approximately 20 dB less noise. For frequencies where both methods produce a source spectrum, they coincide.

4. Discussion

Case 1 showed that CLEAN-SC can predict arbitrary results at low frequencies. B-CLEAN-SC fixed this by averaging frequency intervals of dirty maps to determine source locations. This works, as the locations of side- and grating-lobes change with frequency so that they cancel out during the averaging. Additionally, the source location at low frequencies below the Rayleigh resolution limit is determined based on higher frequencies, where the source positions can still be resolved. The case showed that B-CLEAN-SC also works for sources with a frequency-dependent spectrum and smallband sources. Here, the initial source marker is not guaranteed to be located on the dominant source for all frequencies. Thus, B-CLEAN-SC is prone to "confuse" the power contribution of these sources. To relax this problem, a low iteration gain factor of $\alpha = 0.1$ was used. Additionally, using frequency intervals instead of using the whole spectrum further relaxes this issue.

Case 2 showed that B-CLEAN-SC is able to correctly determine the location and power of the sources at low frequencies in an open wind tunnel experiment, and its overall noise level was 6 dB lower compared to CLEAN-SC. The introduced metrics and Table 1 showed that B-CLEAN-SC improves with increasing frequency intervals in spatial and spectral accuracy up to an optimum at 1/4 of the total frequencies, after which spatial accuracy is traded for a deteriorating spectral estimation. One can possibly account for this by defining frequency-dependent intervals so that the intervals are large at low and high frequencies and small at medium frequencies where CLEAN-SC works well. A lower gain factor further relaxes this issue but increases the number of iterations.

Case 3 showed that for a real-world wind tunnel measurement of a Do728, B-CLEAN-SC was able to reconstruct sources throughout the frequency range, compared to CLEAN-SC, which identified sources mainly at $10 \leq He \leq 100$.

Since their location is roughly constant over frequency and corresponds to the geometric features (slat track, flap side edge, etc.), these identified locations are presumably correct. The B-CLEAN-SC result is less noisy compared to the CLEAN-SC result. The ROI PSD showed nearly identical results for both methods in the frequency region where CLEAN-SC correctly identified sources, which was smaller compared to B-CLEAN-SC.

5. Conclusion

This paper presented B-CLEAN-SC, a variation of CLEAN-SC specifically tailored to broadband sources. B-CLEAN-SC assumes that the location of broadband sources is constant over frequency intervals. For synthetic and experimental wind tunnel data, B-CLEAN-SC outperformed CLEAN-SC at low frequencies. For experimental real data, B-CLEAN-SC also resulted in 3 dB less broadband noise throughout the frequency range. On wind tunnel data of a Do728, both methods showed that the source location assumption is valid, improves the spatial estimation of sources, and reduces noise.

The algorithmic difference between CLEAN-SC and B-CLEAN-SC is small. B-CLEAN-SC processes multiple frequencies at once and uses one additional operation per iteration compared to CLEAN-SC. As it requires a lower gain factor, the number of iterations increase inverse proportionally to the gain factor to meet a convergence criterion that is, however, not performance relevant. The necessary memory scales linearly with the number of employed frequencies within the interval compared to standard CLEAN-SC, which, in terms of today's computational capacities, should not be an issue. This makes B-CLEAN-SC a viable method for little computational effort but improved results at low and high frequencies.

AUTHOR DECLARATIONS
Conflict of Interest

The author declares that he has no conflict of interest.

DATA AVAILABILITY

The data that support the findings of this study are available from the corresponding author upon reasonable request.

References

Ahlefeldt, T. (**2013**). "Aeroacoustic measurements of a scaled half-model at high Reynolds numbers," AIAA J. **51**(12), 2783–2791.

Ahlefeldt, T. (**2017**). "Microphone array measurement in European transonic wind tunnel at flight Reynolds numbers," AIAA J. **55**, 36–48.

Ahlefeldt, T., Ernst, D., Goudarzi, A., Raumer, H.-G., and Spehr, C. (**2023**). "Aeroacoustic testing on a full aircraft model at high Reynolds numbers in the European transonic windtunnel," J. Sound Vib. **566**, 117926.

Brooks, T. F., and Humphreys, W. M. (**2006**). "A deconvolution approach for the mapping of acoustic sources (DAMAS) determined from phased microphone arrays," J. Sound Vib. **294**(4–5), 856–879.

Chardon, G. (**2023**). "Gridless covariance matrix fitting methods for three dimensional acoustical source localization," J. Sound Vib. **551**, 117608.

Chardon, G., Picheral, J., and Ollivier, F. (**2021**). "Theoretical analysis of the DAMAS algorithm and efficient implementation of the covariance matrix fitting method for large-scale problems," J. Sound Vib. **508**, 116208.

Ehrenfried, K., and Koop, L. (**2007**). "Comparison of iterative deconvolution algorithms for the mapping of acoustic sources," AIAA J. **45**(7), 1584–1595.

Goudarzi, A. (**2022**). "Frequency domain beamforming using neuronal networks," in *Proceedings of the 9th Berlin Beamforming Conference 2022 (BeBeC)*, June 9–10, Berlin, Germany, available at https://www.bebec.eu/fileadmin/bebec/downloads/bebec-2022/papers/BeBeC-2022-S02.pdf.

Goudarzi, A. (**2023**). "Global, and local optimization beamforming for broadband sources," arXiv:2211.04921.

Goudarzi, A., Spehr, C., and Herbold, S. (**2021**). "Automatic source localization and spectra generation from sparse beamforming maps," J. Acoust. Soc. Am. **150**(3), 1866–1882.

Kujawski, A., and Sarradj, E. (**2022**). "Fast grid-free strength mapping of multiple sound sources from microphone array data using a transformer architecture," J. Acoust. Soc. Am. **152**(5), 2543–2556.

Malgoezar, A. M. N., Snellen, M., Merino-Martinez, R., Simons, D. G., and Sijtsma, P. (**2017**). "On the use of global optimization methods for acoustic source mapping," J. Acoust. Soc. Am. **141**(1), 453–465.

Merino-Martínez, R., Luesutthiviboon, S., Zamponi, R., Carpio, A. R., Ragni, D., Sijtsma, P., Snellen, M., and Schram, C. (**2020**). "Assessment of the accuracy of microphone array methods for aeroacoustic measurements," J. Sound Vib. **470**, 115176.

Merino-Martínez, R., Sijtsma, P., Snellen, M., Ahlefeldt, T., Antoni, J., Bahr, C. J., Blacodon, D., Ernst, D., Finez, A., Funke, S., Geyer, T. F., Haxter, S., Herold, G., Huang, X., Humphreys, W. M., Leclère, Q., Malgoezar, A., Michel, U., Padois, T., Pereira, A., Picard, C., Sarradj, E., Siller, H., Simons, D. G., and Spehr, C. (**2019**). "A review of acoustic imaging methods using phased microphone arrays," CEAS Aeronaut. J. **10**(1), 197–230.

Sarradj, E. (**2012**). "Three-dimensional acoustic source mapping with different beamforming steering vector formulations," Adv. Acoust. Vib. **2012**, 1–12.

Sarradj, E. (**2022**). "Three-dimensional gridless source mapping using a signal subspace approach," in *Proceedings of the 9th Berlin Beamforming Conference 2022 (BeBeC)*, June 9–10, Berlin, Germany, available at https://www.bebec.eu/fileadmin/bebec/downloads/bebec-2022/papers/BeBeC-2022-S06.pdf.

Sijtsma, P. (**2007**). "Clean based on spatial source coherence," Int. J. Aeroacoust. **6**, 357–374.

Sijtsma, P., Merino-Martinez, R., Malgoezar, A. M., and Snellen, M. (**2017**). "High-resolution CLEAN-SC: Theory and experimental validation," Int. J. Aeroacoust. **16**(4–5), 274–298.